

Wireless Electronic Skin with Integrated Pressure and Optical Proximity Sensing

Eric J. Markvicka, Jonathan M. Rogers, and Carmel Majidi

Abstract—Electronic skins and tactile sensors can provide the sense of touch to robotic manipulators. These sensing modalities complement existing long range optical sensors and can provide detailed information before and after contact. However, integration with existing systems can be challenging due to size constraints, the interface geometry, and restrictions of external wiring used to interface with the sensor. Here, we introduce a low-profile, wireless electronic skin for direct integration with existing robotic manipulators. The flexible electronic skin combines pressure, optical proximity sensing, and a micro-LIDAR device in a small, low profile package. Each of the sensors are characterized individually and the system is demonstrated on Robonaut 2, an anthropomorphic robot designed to work in environments designed for humans. We demonstrate the sensor can be used for contact sensing, mapping of local unknown environments, and to provide medical monitoring during an emergency in a remote area.

I. INTRODUCTION

As highly specialized robots move out of the factories and into our homes they will be required to perform a multitude of tasks [1], [2]. This shift from specialized to general purpose robots requires the integration of sensors to provide information for object detection, recognition, and localization and integration with advanced algorithms to interpret these data streams. While long range optical sensors have enabled mobile robots to autonomously navigate in a variety of environments, robotic manipulators often have difficulty manipulating objects because of the large uncertainty due to the lack of resolution.

For unstructured manipulation tasks, humans far exceed the capabilities of robotic manipulators. During manipulation, human skin plays an especially critical role in providing rich information about physical properties and contact, while human vision only provides indirect information [3]. Mimicking human skin for tactile sensing is a grand challenge that could provide robots with sensory perception that potentially matches or exceeds the performance of natural human manipulation [4]. While there has been significant development of artificial tactile sensors [5], [6], [7], and even commercial products [8], tactile sensors are rarely deployed in practice [9].

Here, we present a compact, low profile electronic skin with miniaturize multimodal sensor node ($14.2 \times 7 \times 2$ mm)

E. J. Markvicka and C. Majidi are with the Soft Machines Lab, Robotics Institute, Carnegie Mellon University, Pittsburgh, PA 15213

E. J. Markvicka is currently with the Smart Materials and Robotics Laboratory, Department of Mechanical and Materials Engineering, University of Nebraska–Lincoln, Lincoln, NE 68588 eric.markvicka@unl.edu

J. M. Rogers is with NASA Johnson Space Center, Houston, TX 77058

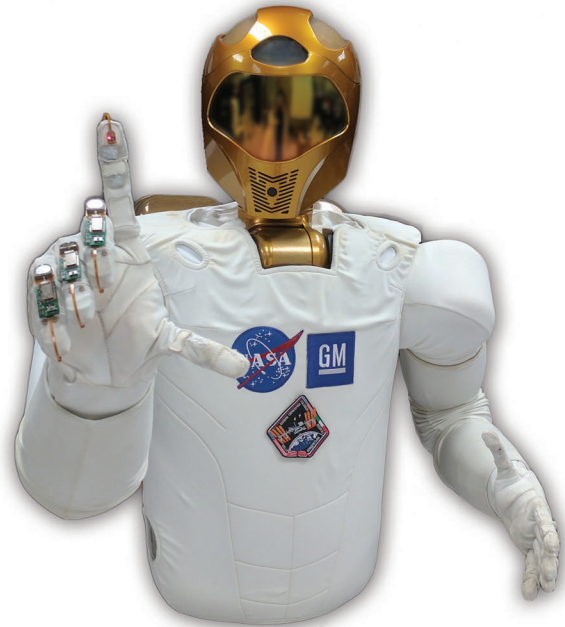


Fig. 1. Robonaut 2 augmented with the wireless electronic skin for pressure and optical proximity sensing. The sensor is attached to each finger on the inner distal phalanx, with wireless control board and battery attached to the exterior of the phalange.

for integration with existing robotic manipulators. The sensor node combines low-power integrated circuits on a flexible printed circuit board (PCB) for pressure and optical proximity sensing. A custom wireless control board is coupled with the sensor node for signal processing, power regulation, and wireless transmission of data. Each of the sensors are individually characterized and the system is integrated with an existing robotic manipulator. The robotic experiments were performed at the NASA Johnson Space Center in Houston, TX with Robonaut 2 (R2), a humanoid robot designed to work in environments designed for humans [2]. The tactile sensor enables R2 to perform proximity and contact sensing, perform local environment mapping, and take the vital signs of a human. Although the focus here is a hardware implementation, the electronic skin could function as a testbed to evaluate and improve algorithms for online grasp adjustment [10], slip detection [11], or state estimation [12].

II. RELATED WORK

Electronic skins and tactile sensors are used in robotic manipulation to provide information about physical contact,

external stimulation, and environmental conditions. In manipulation, integrated sensors can measure physical properties (hardness, shape, texture) and contact (force, position) and can be used as control parameters in manipulation algorithms to provide real time feedback. Several researchers have developed pressure and contact sensors for robot manipulators based on different transduction mechanisms, including resistive [8], [13], [7], piezoresistive [14], [15], [13], capacitive [16], magnetic [17], [18], and optical [19], [20], [21], [6], [22], [23]. Others have created multi-modal sensors to provide feedback on a range of stimuli include tactile, temperature, proximity, and orientation [24], [25], [26], [27], [28], [13], [15], [29]. While contact sensors in unstructured environments would provide valuable information about the uncertainty of contact or material properties, they are rarely used in practice [9]. Nonetheless, since the 1970s there has been continued interest in developing new and innovative sensors for integration with robotic manipulators [30], including efforts to introduce commercial products [8], [14].

Proximity sensors can provide information before contact occurs and be used to provide information about the objects properties or estimation of location. One limitation of many previously reported proximity sensors is the dependence on bulk material or surface properties, making it difficult to calculate absolute distance from the sensor. The response of light reflectance sensors are highly non-linear and depend on surface reflectivity, orientation, and texture [20], [21]. Capacitive and inductive proximity sensing depends on the bulk material properties (conductivity) [31]. Mechanical displacement can also be used to detect proximity but this approach requires contact and therefore is also dependent on material properties (stiffness) [19].

Recently, researchers have placed cameras at the point of manipulation to provide rich information about the object such as force, texture, or hardness using specialized lighting and reflective coatings [32], [33]. Similarly, transparent films with markers provide information before and after contact [34]. While these approaches provide rich information during manipulation they are computationally expensive and sacrifice dexterity because of the relatively large overall size of the sensor. Recent efforts have focused on reducing the thickness of camera-based sensors [35].

In general, there has been significant advancements towards developing electronic skins and tactile sensors to improve the capability of robotic manipulation systems. However, further progress depends on “sticker-like” hardware architectures that are flexible and wireless so that they can be easily incorporated into existing robotic hands without requiring modifications or complete replacement of the robotic hand and/or fingers [36]. Here, we address this by presenting a low-profile, wireless electronic skin to enable integration with existing systems and dexterous robotic hands.

III. WIRELESS ELECTRONIC SKIN DESIGN

Sensorized electronic skins can provide the sense of touch to existing robotic systems. However, integration with existing systems can be challenging. For integration with

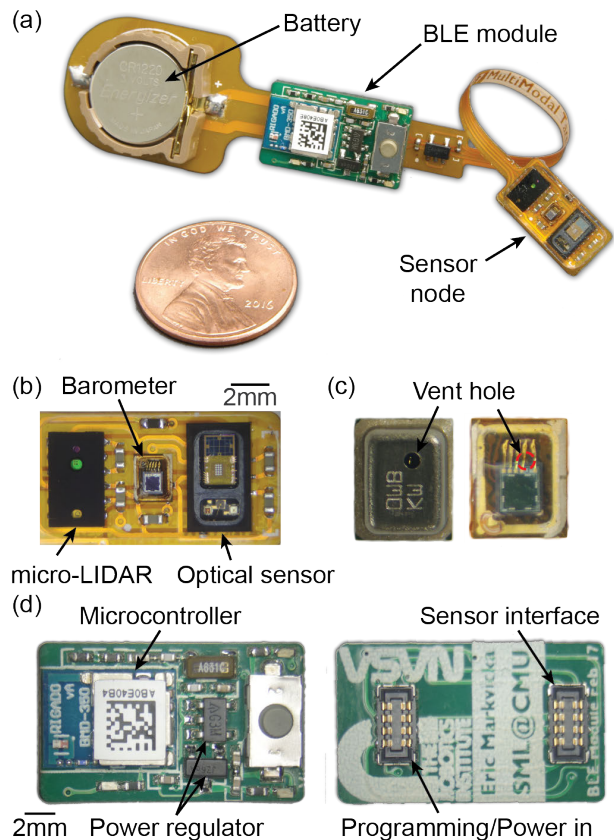


Fig. 2. Tactile sensor with wireless control board. (a) Photograph of tactile sensor with wireless control board and coin cell battery. (b) Magnified photograph of the sensor node. (c) Magnified photograph of the barometer with and without the metal cover. (d) Photographs of the wireless control board.

existing robotic hands and fingers, the electronic skin must be thin, flexible and capable of conforming to curved surfaces. In addition, the amount of wiring required to power and communicate with the sensing skin should be minimized. While, two-wire serial communication protocols (*e.g.* I2C and TWI) can reduce the number of wires, any external wires can potentially limit the overall kinematics or dexterity of existing robotic systems.

Here, we present a low-profile, wireless electronic skin that combines a sensor node, Bluetooth low energy (BLE) module for data processing and wireless communication, and battery to provide a wire-free solution for integration with existing systems (Fig. 2). The sensor node combines a pressure sensor, high-sensitivity optical sensor, and micro-LIDAR distance sensor (Fig. 2b). The relevant sensor parameters are provided in Table I. This section provides an overview of the design of the wireless electronic skin.

A. Pressure Sensor

For contact sensing, we selected a barometer (BMP280, Bosch) with high accuracy and long term stability that can be sampled at a rate up to 157 Hz. The sensor has a high resolution, small footprint, and low power consumption. To prepare the barometer, the integrated circuit (IC) is first soldered to a rigid PCB, a silicone elastomer (PDMS;

Sylgard 184, Dow Corning; mixed at a 10:1 oligomer-to-curing agent ratio) is poured over the barometer, and is immediately placed in a vacuum chamber for 30 minutes to remove any air trapped under the metal cover. After degassing, the elastomer is then fully cured in a 100°C oven for 1 hour. After curing, the elastomer is peeled off the outside of the barometer and the cover is carefully removed by applying a small torsional load using jewelers pliers to break the adhesive bond between the metal cover and mounting package. The cover is removed because the vent hole is not directly over the silicon diaphragm (Fig. 2c). The barometer is then desoldered from the rigid PCB, soldered to the flex PCB sensor node using a reflow soldering oven, and a final layer of PDMS is cast over the sensor array using a two-part acrylic mold (thickness = 1.5 mm).

TABLE I

RELEVANT SENSOR PARAMETERS.			
Sensor	Range	Resolution	Frequency
Pressure Sensor (BMP280)	30-170 kPa	± 0.16 Pa	1-157 Hz
Optical Sensor (MAX30105)	—	18-bit (ADC)	50-3200 Hz
Micro-LIDAR (VL6180x)	5-200 mm	± 1 mm	14-118 Hz

B. Optical Proximity Sensor

Optical proximity sensors are generally highly dependent on the surface (reflectance sensors) or bulk (inductive, capacitive) material properties of the object; require dense features (computer vision) or contact (mechanical displacement); or have limited sampling rates to sense proximity. Here we integrate a high-sensitivity, high frequency reflective optical sensor and an absolute range sensing, low frequency micro-LIDAR distance sensor and directly compare the properties of these two sensing modalities (Table I). The high-sensitivity reflective optical sensor (MAX30105, Maxim Integrated) includes three internal LEDs (green, red, and infrared) and photodetector to measure the amount of reflected light. The sensor can also be used for smoke and particle detection and photoplethysmography to monitor heart rate or blood oxygen saturation. Instead of measuring the amount of light reflected back from the object, the micro-LIDAR sensor (VL6180x, STMicroelectronics) measures absolute distance by measuring the time the light takes to travel to the nearest object and reflect back to the sensor (time-of-flight).

C. Signal Processing and Wireless communication

The custom BLE module is used to collect, process, and transmit the signals from the sensor node (Fig. 2). The control board is built around an ultra-low power BLE SoC with Cortex-M4F processor (nRF52, Nordic). For connection to an Android device, up to 15 electronic skins can be connected with concurrent active notifications. For connection to a computer, most BLE dongles can simultaneously connect to at least 6 devices, requiring one dongle per hand. The low-energy, BLE communication has a maximum data throughput of 1 Mbps. The control board also includes power management circuitry (3v, 1.8v) and low profile board-to-board

connectors to interface with the tactile sensor and battery (CR1220). The coin cell battery provides power for at least one hour of continuous operation. The micro-LIDAR device requires more current than the coin cell battery can supply. A lithium ion polymer battery (3.7v) was used for all absolute range sensing experiments. The sensor data is read from the sensor's internal buffer at 20 Hz and wirelessly transmitted to a desktop computer or mobile computing device using the Bluetooth Low Energy (BLE) protocol. The data is then locally processed, plotted in a graphical user interface (GUI), and locally stored. For time sensitive applications (e.g., slip detection), the collection frequency can be increased and for higher bandwidth communication, other RF options should be considered such as WiFi. Additional time synchronization methods would be required to eliminate timing drift between electronic skins.

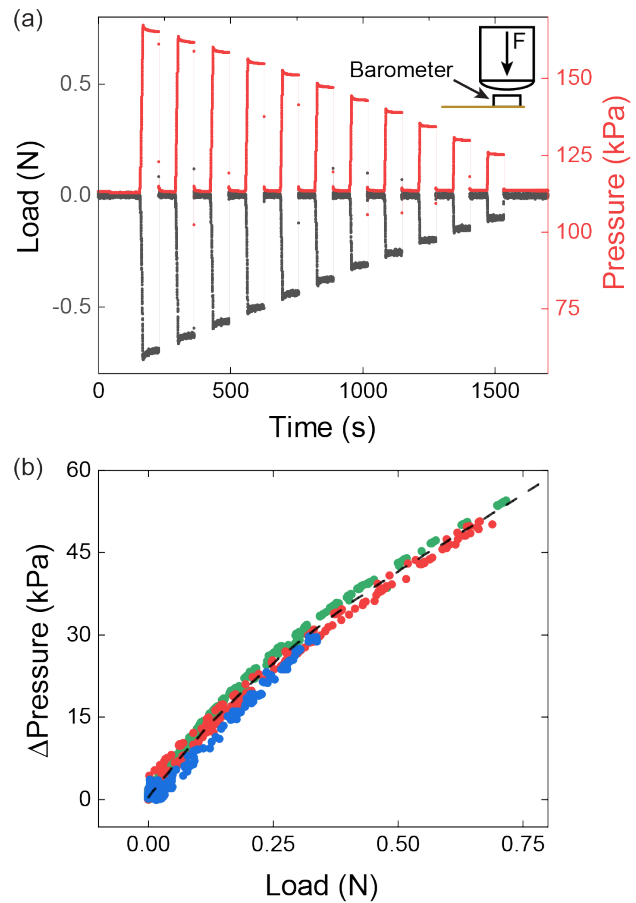


Fig. 3. Characterization of barometer embedded in elastomer. (a) Sensor is subjected to a compressive loading and hold deformation profile (-0.7 to -0.1 N) and displays minimal drift under constant loading. (b) 2,000 points are randomly selected from the cyclic loading experiment and plotted as a function of applied load (n=3).

IV. CALIBRATION

A. Contact sensing

The pressure sensor was subjected to a compressive load and hold deformation profile (-0.7 to -0.1 N), as shown in Fig. 3a. The compressive load was applied by a material testing machine (5969, Instron) using a 3 inch hemispherical,

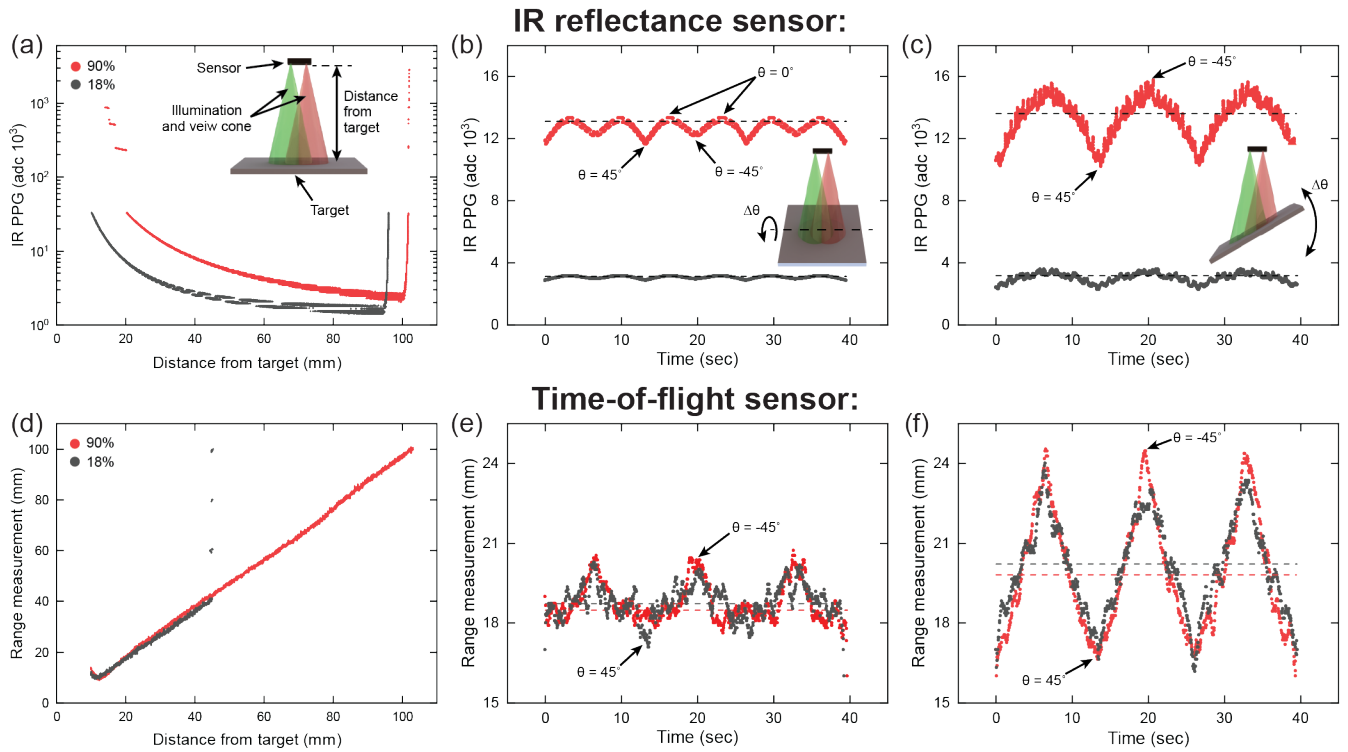


Fig. 4. Characterization of optical sensors. (a-c) Response of the IR reflectance sensor as a function of (a) distance from the target, (b) orientation of the target with the rotation axis parallel to the sensor, and (c) orientation of the target with the rotation axis perpendicular to the sensor. (d-f) Response of the micro-LIDAR sensor as a function of (d) distance from the target, (e) orientation of the target with the rotation axis parallel to the sensor, and (f) orientation of the target with the rotation axis perpendicular to the sensor. (b,c,e,f) Three cycles are shown, where the dashed line is the sensor response when the target is parallel to the sensor. For each experiment, two targets with different surface reflectance (90% (red) and 18% (gray)) were used. The y-axis of (a) is plotted on a log scale.

silicone elastomer indenter (PDMS, Sylgard 184 mixed at a 10:1 oligomer-to-curing agent ratio, Dow Corning). A hemispherical indenter was selected to ensure consistent and repeated contact between the sensor and material testing machine. Although the barometer is calibrated at the factory, each barometer had a different baseline pressure. Moreover, this baseline pressure changes when the chip is modified for integration with the electronic skin. To account for this difference in baseline pressure, the change in pressure ($\Delta P = P - P_0$) until saturation (~ 170 kPa) was plotted as a function of applied load and a cubic curve was fit to the data ($y = 0.05x^3 - 0.1x^2 + 0.12x$, $R^2 = 0.99$; Fig. 3b). The nonlinear response is likely due to the hemispherical shape of the indenter, which, according to Hertzian contact theory leads to a cubic relationship between applied force and internal pressure centered above the point of contact [37].

This experiment demonstrates the fast response, negligible hysteresis, and repeatability between fabricated pressure sensors. To provide an accurate estimation of force, the pressure distribution would need to be known. A constant contact area could be prescribed by including a rigid plate above the pressure sensor. However, the rigid plate would negatively influence the flexibility of the electronic skin and non-axial forces would result in tilting of the rigid plate and uneven pressure applied to the sensor. Additional characterization would be required to fully characterize the sensor for all potential loading conditions.

B. Optical Proximity sensor

The high-sensitivity optical sensor is directly compared to the micro-LIDAR device. Sensor characterization is performed as a function of distance from the sensor and the influence of the orientation of the target for a fixed distance. The sensor response is compared for two surfaces with different surface reflectance (18%, 90%, Kodak R-27). The results are shown in Fig. 4.

To measure the sensor response as a function of the distance, the target was mounted to the traveling head of a material testing machine and displaced at a constant velocity (100 mm \cdot min $^{-1}$). The high-resolution optical sensor displayed the largest change in response and could be collected at high frequencies (up to 3.2 kHz). However, the response was highly nonlinear and dependent on the surface reflectance (Fig. 4a). For characterization, data was sampled at 1.6 kHz and each 8 adjacent samples were averaged to reduce the amount of data throughput and energy consumption. Here, we only included the results from the infrared (IR) LED, because the green and red LED had a similar response. The micro-LIDAR sensor response was then characterized. The sensor response is linear, a direct measurement of distance, and is observed to be independent of surface reflectance. However, the measurement convergence time (8 to 71 ms) is a function of the distance from the sensor and the surface reflectance, which limits the collection frequency

(Fig. 4b). For characterization, the maximum measurement convergence time was set to 50 ms (20 Hz). As compared to the IR reflectance sensor, the micro-LIDAR sensor had a lower resolution (± 1 mm).

To measure the influence of surface orientation, the target was mounted approximately 20 mm from the sensor and a servo actuator (AX-12A, Dynamixel) was used to rotate the target (-45° to 45°) at a constant angular velocity (0.25 rad \cdot sec $^{-1}$). Two different conditions were characterized 1) the axis of rotation was parallel to the sensor and 2) the axis of rotation was perpendicular to the sensor. A precision linear stage (460A-X, Newport) was used to center the sensor over the axis of rotation. First, the dependence on orientation with the emitter and detector coincident with the axis of rotation, where the long axis of the chip was parallel to the axis of rotation was characterized (Fig. 4b, 4e). The response of the optical reflectance sensor was maximum when the target was parallel to the sensor and was reduced as the rotation angle increased or decreased (Fig. 4b). The non-symmetry between positive and negative rotation could be an artifact of misalignment with the axis of rotation. The micro-LIDAR sensor also exhibited a dependence on the orientation of the target (Fig. 4e), yet the signal response was within the noise of the sensor (± 1 mm). The actual distance from the target (dashed line in Fig. 4e) was similar to the average of the recorded signal.

Next, the dependence on orientation perpendicular to the sensor was characterized (Fig. 4c, 4f). The response of the optical reflectance sensor was maximum when the target was closest to the photodetector ($\theta = -45^\circ$) and monotonically decreased to $\theta = 45^\circ$ (Fig. 4c). The micro-LIDAR sensor response was similar to the reflectance sensor and was maximum when the target was closest to the detector (Fig. 4e). For both sensors, we observed a dependence on the orientation perpendicular to the sensor. The combination of sensors could potentially be used to determine the orientation of a flat surface.

V. APPLICATION

The wireless electronic skin was integrated with Robonaut 2 (R2) to evaluate the sensor on an existing robotic platform. All experiments with R2 were performed at the NASA Johnson Space Center in Houston, TX. The tactile sensor was adhesively attached to the exterior of the soft goods (*i.e.* textiles) on the inner distal phalanx of the fingers of the robotic hand using double sided tape (VHB, 3M), as shown in Fig. 1. The wireless control board and battery were adhesively attached to the exterior of the phalange.

A. Contact sensing during manipulation

Data from the pressure sensor was collected while R2 grasped a 9 kg dumbbell weight (Fig. 5). All four fingers contacted the foam-padded bar of the weight and the detection of contact is shown in Fig. 5 (inset). The fingertips of Robonaut 2 can exert a force of 2.25 kg while fully extended [38]. While the selected pressure sensor is adequate for forces generated in normal manipulation tasks (15-90 g)

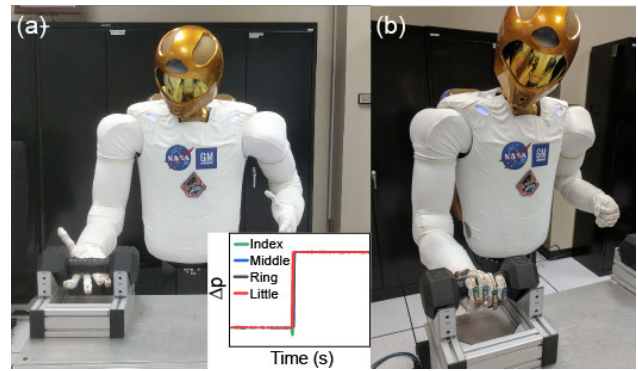


Fig. 5. Contact sensing during manipulation. Photograph sequence of Robonaut 2 (a) positioning hand and (b) grasping a dumbbell weight. (inset) Signal response of the contact sensors on each of the fingers, before and after contact. Robonaut 2 is able to generate a significant amount of fingertip force and the sensors almost immediately saturate but continue operating after contact.

[5], the barometer is quickly saturated during a power grasp. This experiment demonstrates that the barometer can survive larger contact forces. A barometer with higher absolute pressure range could have been selected. However, they're often larger in overall size and have reduced sensitivity.

B. Local environment mapping

In addition to proximity detection, the optical proximity sensors can be used to map a local environment. A toy model of the Space Shuttle orbiter was scanned using the micro-LIDAR device to demonstrate the ability to map an object with variable surface properties (reflectivity, orientation). Nine horizontal scans were captured at a constant velocity (20 mm \cdot s $^{-1}$) using the micro-LIDAR sensor (Fig. 6a). The sensor response as a function of time is shown in Fig. 6b, 6c. To improve visualization, the sensor response is plotted as measured height instead of distance from the sensor. Different components of the orbiter can be identified in the horizontal scans such as the fuselage, wing, and vertical stabilizer, while the changes in surface or bulk material properties are not apparent. The measured height of the fuselage (black cloth floor to top of fuselage) is comparable to the actual measured height (50 mm). The x-axis of the individual scans were synced using the midpoint of the half-height width for the peak with maximum prominence.

C. Telemedicine: robotic vital sign monitoring

In the event of a medical emergency in a remote area, such as the International Space Station or deep space flight, R2 could collect photoplethysmogram (PPG) waveforms to monitor the vitals signs of an astronaut using the high-resolution optical proximity sensor (Fig. 7). To collect the PPG waveforms, R2 made contact with the index finger of a human and recorded the reflected light from the IR and red LED. The data from the pressure sensor was also collected to ensure sufficient contact was maintained [39]. A subset of the data that was collected is shown in Fig. 7c. The data from the pressure sensor indicates relative motion between the robot and human. Heart rate is estimated by taking the Fast

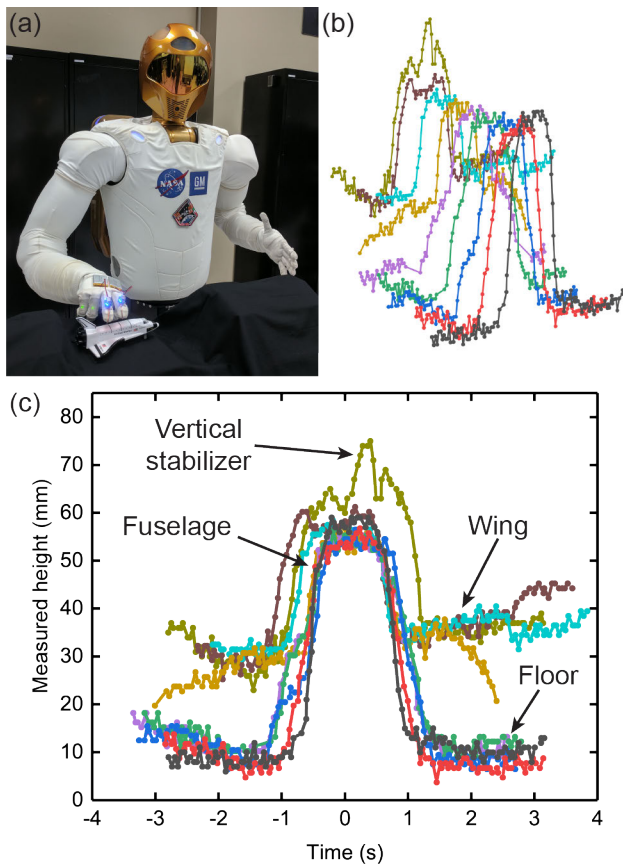


Fig. 6. Local environment mapping. (a) Photograph of Robonaut 2 scanning a toy model of the Space Shuttle orbiter. (b-c) Isometric and front view of the data from the micro-LIDAR sensor on the index finger. Horizontal sweeps across the orbiter were completed at a constant velocity. General components of the orbiter can be identified from the scans such as the fuselage, wing, and vertical stabilizer. Lines are included between data points to help guide the eyes of the reader.

Fourier Transform (Fig. 7b) of the IR signal and the dominant frequency between between 0.5 Hz (30 BPM) and 10 Hz (600 BPM) is selected. The dominant frequency corresponds to a heart rate of 80 BPM.

VI. CONCLUSIONS

A low-profile, wireless electronic skin was developed for integration with existing robotic manipulators. The multi-modal sensor node provides rich information before and after contact including absolute distance, contact detection, and photoplethysmogram waveforms. The wireless connectivity of the electronic skin eliminates wires for power and data transmission. As compared to the reflective optical proximity sensor, the micro-LIDAR device provides improvements in terms of range sensing and enables local mapping of an unknown object. However, the sensor has reduced sensitivity and bandwidth. The optical proximity sensor can be used to collect photoplethysmogram waveforms to estimate human vital signs such as heart rate in a remote area. The direct integration of an absolute range sensor and reflective light sensor could allow the system to reason about surface properties such as reflectance, texture, or orientation to

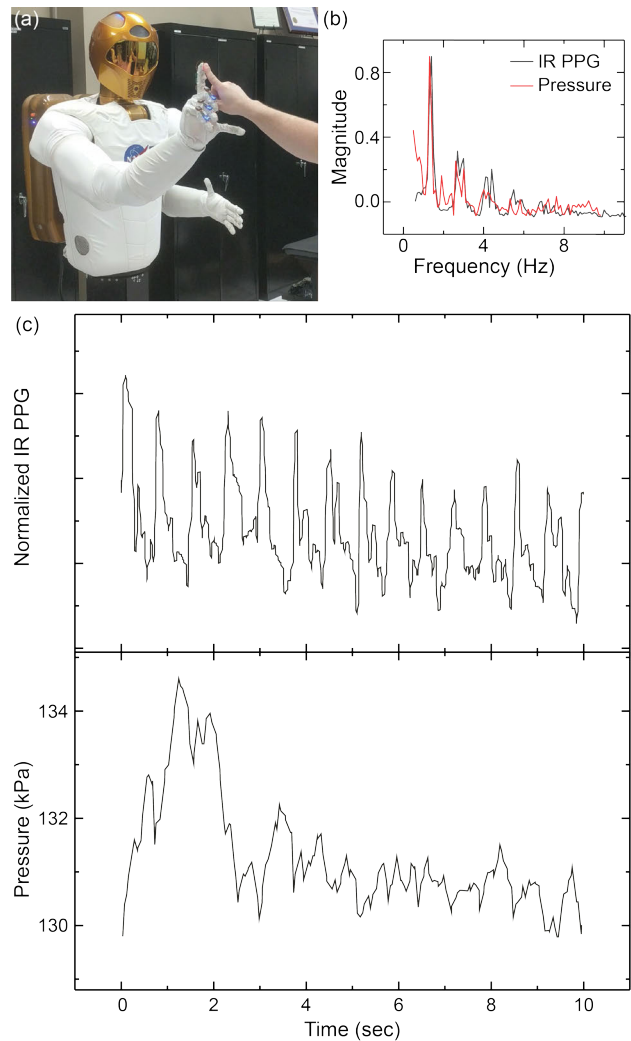


Fig. 7. Telemedicine: robotic vital sign monitoring. (a) Photograph of Robonaut 2 recording human physiological data from the index finger of a human. (b) FFT of photoplethysmogram (PPG) and pressure waveforms. The dominant frequency (0.5-10 Hz; 30-600 BPM) can be used to estimate heart rate. (c) Plot of IR PPG waveform and arterial pressure pulse versus time, measured at the fingertip. The relative motion between the human and robot is reflected in the pressure waveform.

improve the accuracy of the distance measurement. Finally, the wireless electronic skin was integrated with Robonaut 2 to demonstrate the capabilities and ease of integration with an existing robotic manipulation platform. Future work includes integration with other existing robotic platforms and algorithms to improve dexterous manipulation.

ACKNOWLEDGMENT

The authors acknowledge support from the NASA Early Career Faculty Award (NNX14AO49G; Research Collaborator: Dr. Bill Bluethmann). Sensor and mechanical characterization was performed on equipment supported through an Office of Naval Research (ONR) Defense University Research Instrumentation Program (DURIP) (Bioinspired Autonomous Systems; Dr. Tom McKenna; N00014140778).

REFERENCES

- [1] S. S. Srinivasa, D. Berenson, M. Cakmak, A. Collet, M. R. Dogar, A. D. Dragan, R. A. Knepper, T. Niemueller, K. Strabala, M. V.

- Weghe, *et al.*, “Herb 2.0: Lessons learned from developing a mobile manipulator for the home,” *Proceedings of the IEEE*, vol. 100, no. 8, pp. 2410–2428, 2012.
- [2] M. A. Diftler, J. Mehling, M. E. Abdallah, N. A. Radford, L. B. Bridgwater, A. M. Sanders, R. S. Askew, D. M. Linn, J. D. Yamokoski, F. Permenter, *et al.*, “Robonaut 2—the first humanoid robot in space,” in *Robotics and Automation (ICRA), 2011 IEEE International Conference on*. IEEE, 2011, pp. 2178–2183.
- [3] R. S. Johansson and J. R. Flanagan, “Coding and use of tactile signals from the fingertips in object manipulation tasks,” *Nature reviews. Neuroscience*, vol. 10, no. 5, p. 345, 2009.
- [4] M. L. Hammock, A. Chortos, B. C.-K. Tee, J. B.-H. Tok, and Z. Bao, “25th anniversary article: the evolution of electronic skin (e-skin): a brief history, design considerations, and recent progress,” *Advanced Materials*, vol. 25, no. 42, pp. 5997–6038, 2013.
- [5] R. S. Dahiya, G. Metta, M. Valle, and G. Sandini, “Tactile sensing—from humans to humanoids,” *IEEE Transactions on Robotics*, vol. 26, no. 1, pp. 1–20, 2010.
- [6] P. Piacenza, K. Behrman, B. Schifferer, I. Kymissis, and M. Ciocarlie, “A sensorized multicurved robot finger with data-driven touch sensing via overlapping light signals,” *IEEE/ASME Transactions on Mechatronics*, pp. 1–1, 2020.
- [7] T. Someya, T. Sekitani, S. Iba, Y. Kato, H. Kawaguchi, and T. Sakurai, “A large-area, flexible pressure sensor matrix with organic field-effect transistors for artificial skin applications,” *Proceedings of the National Academy of Sciences*, vol. 101, no. 27, pp. 9966–9970, 2004.
- [8] J. A. Fishel and G. E. Loeb, “Sensing tactile microvibrations with the biotac—comparison with human sensitivity,” in *Biomedical Robotics and Biomechanics (BioRob), 2012 4th IEEE RAS & EMBS International Conference on*. IEEE, 2012, pp. 1122–1127.
- [9] N. Correll, K. E. Bekris, D. Berenson, O. Brock, A. Causo, K. Hauser, K. Okada, A. Rodriguez, J. M. Romano, and P. R. Wurman, “Analysis and observations from the first amazon picking challenge,” *IEEE Transactions on Automation Science and Engineering*, vol. 15, no. 1, pp. 172–188, 2016.
- [10] R. Patel, R. Cox, B. Romero, and N. Correll, “Improving grasp performance using in-hand proximity and contact sensing,” *arXiv preprint arXiv:1701.06071*, 2017.
- [11] C. Melchiorri, “Slip detection and control using tactile and force sensors,” *IEEE/ASME transactions on mechatronics*, vol. 5, no. 3, pp. 235–243, 2000.
- [12] M. C. Koval, M. R. Dogar, N. S. Pollard, and S. S. Srinivasa, “Pose estimation for contact manipulation with manifold particle filters,” in *Intelligent Robots and Systems (IROS), 2013 IEEE/RSJ International Conference on*. IEEE, 2013, pp. 4541–4548.
- [13] W. W. Lee, Y. J. Tan, H. Yao, S. Li, H. H. See, M. Hon, K. A. Ng, B. Xiong, J. S. Ho, and B. C. Tee, “A neuro-inspired artificial peripheral nervous system for scalable electronic skins,” *Science Robotics*, vol. 4, no. 32, p. eaax2198, 2019.
- [14] Y. Tenzer, L. P. Jentoft, and R. D. Howe, “The feel of MEMS barometers: Inexpensive and easily customized tactile array sensors,” *IEEE Robotics & Automation Magazine*, vol. 21, no. 3, pp. 89–95, 2014.
- [15] T. Hellebrekers, K. B. Ozutemiz, J. Yin, and C. Majidi, “Liquid metal-microelectronics integration for a sensorized soft robot skin,” in *2018 IEEE/RSJ International Conference on Intelligent Robots and Systems (IROS)*. IEEE, 2018, pp. 5924–5929.
- [16] A. Charalambides and S. Bergbreiter, “Rapid manufacturing of mechanoreceptive skins for slip detection in robotic grasping,” *Advanced Materials Technologies*, vol. 2, no. 1, 2017.
- [17] H. Wang, G. De Boer, J. Kow, A. Alazmani, M. Ghajari, R. Hewson, and P. Culmer, “Design methodology for magnetic field-based soft tri-axis tactile sensors,” *Sensors*, vol. 16, no. 9, p. 1356, 2016.
- [18] T. Hellebrekers, O. Kroemer, and C. Majidi, “Soft magnetic skin for continuous deformation sensing,” *Advanced Intelligent Systems*, vol. 1, no. 4, p. 1900025, 2019.
- [19] J. Konstantinova, A. Stilli, and K. Althoefer, “Force and proximity fingertip sensor to enhance grasping perception,” in *Intelligent Robots and Systems (IROS), 2015 IEEE/RSJ International Conference on*. IEEE, 2015, pp. 2118–2123.
- [20] R. Patel and N. Correll, “Integrated force and distance sensing using elastomer-embedded commodity proximity sensors,” in *Robotics: Science and Systems*, 2016.
- [21] K. Hsiao, P. Nangeroni, M. Huber, A. Saxena, and A. Y. Ng, “Reactive grasping using optical proximity sensors,” in *Robotics and Automation, 2009. ICRA’09. IEEE International Conference on*. IEEE, 2009, pp. 2098–2105.
- [22] M. Ramuz, B. C.-K. Tee, J. B.-H. Tok, and Z. Bao, “Transparent, optical, pressure-sensitive artificial skin for large-area stretchable electronics,” *Advanced Materials*, vol. 24, no. 24, pp. 3223–3227, 2012.
- [23] C. To, T. Hellebrekers, J. Jung, S. J. Yoon, and Y.-L. Park, “A soft optical waveguide coupled with fiber optics for dynamic pressure and strain sensing,” *IEEE Robotics and Automation Letters*, vol. 3, no. 4, pp. 3821–3827, 2018.
- [24] T. Bhattacharjee, A. Jain, S. Vaish, M. D. Killpack, and C. C. Kemp, “Tactile sensing over articulated joints with stretchable sensors,” in *2013 World Haptics Conference (WHC)*. IEEE, 2013, pp. 103–108.
- [25] J. Wade, T. Bhattacharjee, R. D. Williams, and C. C. Kemp, “A force and thermal sensing skin for robots in human environments,” *Robotics and Autonomous Systems*, vol. 96, pp. 1–14, 2017.
- [26] T. Someya, Y. Kato, T. Sekitani, S. Iba, Y. Noguchi, Y. Murase, H. Kawaguchi, and T. Sakurai, “Conformable, flexible, large-area networks of pressure and thermal sensors with organic transistor active matrixes,” *Proceedings of the National Academy of Sciences*, vol. 102, no. 35, pp. 12 321–12 325, 2005.
- [27] P. Middendorfer and G. Cheng, “3d surface reconstruction for robotic body parts with artificial skins,” in *2012 IEEE/RSJ International Conference on Intelligent Robots and Systems*. IEEE, 2012, pp. 4505–4510.
- [28] P. Middendorfer, E. Yoshida, and G. Cheng, “Realizing whole-body tactile interactions with a self-organizing, multi-modal artificial skin on a humanoid robot,” *Advanced Robotics*, vol. 29, no. 1, pp. 51–67, 2015.
- [29] S. Denei, P. Maiolino, E. Baglini, and G. Cannata, “Development of an integrated tactile sensor system for clothes manipulation and classification using industrial grippers,” *IEEE Sensors Journal*, vol. 17, no. 19, pp. 6385–6396, 2017.
- [30] H. R. Nicholls and M. H. Lee, “A survey of robot tactile sensing technology,” *The International Journal of Robotics Research*, vol. 8, no. 3, pp. 3–30, 1989.
- [31] D. Göger, H. Alagi, and H. Wörn, “Tactile proximity sensors for robotic applications,” in *Industrial Technology (ICIT), 2013 IEEE International Conference on*. IEEE, 2013, pp. 978–983.
- [32] R. Li, R. Platt, W. Yuan, A. ten Pas, N. Roscup, M. A. Srinivasan, and E. Adelson, “Localization and manipulation of small parts using GelSight tactile sensing,” in *Intelligent Robots and Systems (IROS 2014), 2014 IEEE/RSJ International Conference on*. IEEE, 2014, pp. 3988–3993.
- [33] W. Yuan, C. Zhu, A. Owens, M. A. Srinivasan, and E. H. Adelson, “Shape-independent hardness estimation using deep learning and a GelSight tactile sensor,” *arXiv preprint arXiv:1704.03955*, 2017.
- [34] A. Yamaguchi and C. G. Atkeson, “Combining finger vision and optical tactile sensing: Reducing and handling errors while cutting vegetables,” in *Humanoid Robots (Humanoids), 2016 IEEE-RAS 16th International Conference on*. IEEE, 2016, pp. 1045–1051.
- [35] E. Donlon, S. Dong, M. Liu, J. Li, E. Adelson, and A. Rodriguez, “Gelslim: A high-resolution, compact, robust, and calibrated tactile-sensing finger,” in *2018 IEEE/RSJ International Conference on Intelligent Robots and Systems (IROS)*. IEEE, 2018, pp. 1927–1934.
- [36] E. Markvicka, G. Wang, Y.-C. Lee, G. Laput, C. Majidi, and L. Yao, “Electrodermis: Fully untethered, stretchable, and highly-customizable electronic bandages,” in *Proceedings of the 2019 CHI Conference on Human Factors in Computing Systems*, 2019, pp. 1–10.
- [37] K. Johnson, *Contact Mechanics*. Cambridge University Press, 1985. [Online]. Available: <https://books.google.com/books?id=ACxsQgAACAAJ>
- [38] L. B. Bridgwater, C. Ihrke, M. A. Diftler, M. E. Abdallah, N. A. Radford, J. Rogers, S. Yayathi, R. S. Askew, and D. M. Linn, “The Robonaut 2 hand-designed to do work with tools,” in *Robotics and Automation (ICRA), 2012 IEEE International Conference on*. IEEE, 2012, pp. 3425–3430.
- [39] R. P. Dresher and Y. Mendelson, “Reflectance forehead pulse oximetry: Effects of contact pressure during walking,” in *2006 International Conference of the IEEE Engineering in Medicine and Biology Society*. IEEE, 2006, pp. 3529–3532.